ON INTENSITY LIMITATIONS IMPOSED BY TRANSVERSE SPACE-CHARGE EFFECTS IN CIRCULAR PARTICLE ACCELERATORS

L. J. Laslett
Lawrence Radiation Laboratory

Contents

ON INTENSITY LIMITATIONS IMPOSED BY TRANSVERSE SPACE-CHARGE EFFECTS IN CIRCULAR PARTICLE ACCELERATORS

L. J. Laslett
Lawrence Radiation Laboratory

I. Introduction

The influence of space-charge forces on the frequency of betatron oscillations has been recognized for many years as one mechanism which will impose a limit on the number of particles that can be accommodated within a circular accelerator. The implications of the space-charge forces which act on an individual particle have been discussed in several early papers[1-3] and in a recent report by Teng.[4] Attention has also been directed by a number of workers, in particular by members of the Midwestern Universities Research Association staff, to the importance of image forces in this phenomenon.[5]

The intensity limit which arises because of the transverse space-charge effect has provided a powerful argument for the use of high-energy injection, since, because of the almost complete cancellation of the electric and magnetic forces when the effect of image fields may be neglected, the number

---

1. D.W. Kerst, Phys. Rev. 60, 47 (1941).
2. J.P. Blewett, Phys. Rev. 69, 87 (1946).
3. D.L. Judd, "A Study of the Injection Process in Betatrons and Synchrotrons", California Institute of Technology thesis (Pasadena, 1950).
4. L.C. Teng, "Transverse Space-Charge Effects", Argonne National Laboratory Report ANLAD-59 (Argonne, Illinois; February 1, 1963). The papers presented on August 26 by Drs. Lloyd Smith and P. Lapostolle at the 1963 International Accelerator Conference at Dubna are of interest for obtaining self-consistent solutions to the transverse space-charge behavior of a particle beam.
5. See, for example, J. van Bladel, "Image Forces in the Third MURA Model", Midwestern Universities Research Association Report MURA-466 (Madison, Wisconsin; June 12, 1959).

of particles which can be accepted is proportional to $\beta^2\gamma^3$. As we shall see, however, image forces can distort this energy dependence when the ratio of the aperture to the transverse beam dimensions becomes comparable to or less than γ, and the limit to the number of particles will become proportional to γ at high energies. In seeking the attainment of high intensity by means of high-energy injection, therefore, one must employ a sufficiently large aperture to insure that image effects are suppressed or inject at an energy considerably higher than would be required if image effects were negligible. In practice, a careful optimization of the design would be appropriate in order to achieve the best balance between aperture and injection energy for achievement of the desired intensity.

In addition to the space-charge forces which act on an individual particle in the beam, a second phenomenon, involving the transverse movement of the beam as a whole, may be of importance. This latter effect, which of course arises in its entirety from image forces, could lead to an instability for coherent transverse motion of an intense beam. Because, as will be indicated in greater detail below, the forces which could lead to single-particle or to coherent instability are not identical, it may prove to be quite complicated to provide compensating fields which will suppress both of these phenomena.

In the sections which follow we shall give a general discussion of the transverse space-charge phenomena, as they may affect axial stability in a circular accelerator; present some field coefficients that represent the image effects in certain particular geometrical configurations that are analyzed in the Appendices; and finally give some illustrative numerical examples. The influence of space-charge neutralization is ignored in the present report, in the supposition that the time required for complete

neutralization of the beam normally is long compared to the duration of the injection process. The work reported here has benefited from discussions which the writer has enjoyed with staff of the Brookhaven National Laboratory, the Lawrence Radiation Laboratory, the Midwestern Universities Research Association, and the Stanford Linear Accelerator Center.

II. Transverse Space-Charge Effects -- Axial Stability Limit

A. Single-Particle Stability

1. The Assumed Fields

The electric and magnetic fields which arise from the collective action of a uniform isolated beam of elliptical cross section have been evaluated by Teng.[4] In Gaussian units, the field strengths at a distance y above the center of a beam with semi-major (radial) and semi-minor (axial) axes denoted respectively by a and b are

$$\vec{E}_{\text{unbunched}} = 4\lambda \frac{y}{b(a+b)} \hat{j} \tag{1a}$$

$$\vec{H}_{\text{unbunched}} = -4\lambda\beta \frac{y}{b(a+b)} \hat{i} , \quad (y < b) \tag{1b}$$

for the transverse distribution of density assumed by Teng, where the linear charge density (λ) is related to the number of particles in the beam (N) and to the orbit radius (R) by

$$\lambda = \frac{Ne}{2\pi R} . \tag{2}$$

The fields represented by Equations (1a) and (1b) will be modified by the presence of nearby conducting or ferromagnetic material through the

supplementary effect of so-called image fields. In addition, for a given total number of particles, the peak fields, experienced by some of the particles in the beam, will be enhanced - and the maximum attainable intensity correspondingly reduced - if the beam is bunched azimuthally by action of the rf acceleration system or if significant fine structure is otherwise present in the density distribution.

The beam distribution accordingly will be characterized by a "bunching factor", B ($B \leq 1$) representing the ratio of the average to the maximum linear charge or particle density. The relevant fields for an isolated beam accordingly will be taken as

$$\vec{E} = \vec{E}_{\text{unbunched}} \times (1/B) \; ; \tag{3a}$$

and

$$\vec{H} = \vec{H}_{\text{unbunched}} \times (1/B) \; , \tag{3b}$$

of which

$$\vec{H}_{dc} = \vec{H}_{\text{unbunched}} \tag{3b'}$$

$$\vec{H}_{ac} = \vec{H}_{\text{unbunched}} \times (1/B - 1) \; . \tag{3b"}$$

To each of these fields [(3a), (3b'), and (3b")] must be appended appropriate correction factors to account for the supplemental image fields.

The electrostatic field, $\vec{E}$, will be modified by the presence of a vacuum chamber with conducting walls through the addition of terms which insure that the chamber surface (most simply taken as formed by parallel conducting planes, a distance 2h apart) be an equipotential. Likewise, the dc component of the magnetic field, $\vec{H}_{dc}$, will be modified so as to insure that, if possible, this field is directed perpendicular to the surfaces of ferromagnetic magnet poles (most simply taken as formed by parallel pole surfaces, a distance 2g apart). The ac magnetic fields of the beam

will be influenced by skin-effect currents induced in the conducting walls of the vacuum chamber, so as to result in a net ac field which is tangential to this boundary, and the correction factor required in this case may be expected to be identical to that applicable to the electrostatic field. For a beam of reasonably small transverse dimensions, these various correction fields may be considered as evaluated adequately without regard for the cross-sectional size of the beam, and, for small displacements of the test particle, will give rise to forces proportional to the displacement y.

The fields to be employed in analysis of single-particle stability accordingly will be written

$$\vec{E} = \frac{4\lambda}{B}\left[1 + \epsilon_1 \frac{b(a+b)}{h^2}\right] \frac{y}{b(a+b)} \hat{j} =$$

$$= \frac{2}{\pi}\frac{1}{B}\frac{Ne}{R}\left[1 + \epsilon_1 \frac{b(a+b)}{h^2}\right] \frac{y}{b(a+b)} \hat{j}\,, \qquad (4a)$$

$$\vec{H}_{dc} = -4\lambda\beta\left[1 - \epsilon_2 \frac{b(a+b)}{g^2}\right] \frac{y}{b(a+b)} \hat{i} =$$

$$= -\frac{2}{\pi}\beta\frac{Ne}{R}\left[1 - \epsilon_2 \frac{b(a+b)}{g^2}\right] \frac{y}{b(a+b)} \hat{i}\,, \qquad (4b')$$

and

$$\vec{H}_{ac} = -4\lambda\beta\left(\frac{1}{B} - 1\right)\left[1 + \epsilon_1 \frac{b(a+b)}{h^2}\right] \frac{y}{b(a+b)} \hat{i} =$$

$$= -\frac{2}{\pi}\left(\frac{1}{B} - 1\right)\beta\frac{Ne}{R}\left[1 + \epsilon_1 \frac{b(a+b)}{h^2}\right] \frac{y}{b(a+b)} \hat{i}\,, \qquad (4b'')$$

where ϵ_1 and ϵ_2 are numerical factors for which expressions applicable to specific geometrical configurations of practical interest are given below (sub-section 3) and where the lengths h and g respectively serve to characterize conveniently the semi-apertures of the vacuum chamber and magnet gap.

Because the effect of bunching has been explicitly taken into account in writing Equations (4a-b"), the quantity λ should be taken here as representing the average linear charge density, as given by Eq. (2). It may be remarked that in some configurations of possible practical interest the dc component of the beam also gives rise to an axial magnetic field component which effectively is independent of position; such a field component is not considered to affect directly the frequency of axial betatron oscillations, however, and is not included in Eq. (4b') or in the equation of motion which follows.

2. The Equation of Motion

The linear equation for the steady-state axial betatron oscillation of a test particle in the presence of a beam of N identical particles may be written in the smooth approximation as

$$\frac{d^2y}{d\theta^2} + (n + K_E + K_M + K_S)\, y = 0 , \tag{5}$$

where n is the effective field index of the applied magnetic field and in which

$$K_E = -\frac{2}{\pi}\frac{1}{B}\frac{Nr_pR}{\beta^2\gamma\, b(a+b)}\left[1 + \epsilon_1\frac{b(a+b)}{h^2}\right] \tag{6a}$$

$$K_M = \frac{2}{\pi}\frac{Nr_pR}{\gamma\, b(a+b)}\left[1 - \epsilon_2\frac{b(a+b)}{g^2}\right] \tag{6b}$$

$$K_S = \frac{2}{\pi}\left(\frac{1}{B} - 1\right)\frac{Nr_pR}{\gamma\, b(a+b)}\left[1 + \epsilon_1\frac{b(a+b)}{h^2}\right] , \tag{6c}$$

by use of Equations (4a), (4b'), and (4b"). The coefficients K_E, K_M, and

K_S represent respectively the electrostatic effect of the bunched beam, the effect of the magnetostatic dc component of the beam, and the magnetic effect of the ac component of the beam as modified by the skin-effect currents induced in the chamber surface. The quantity r_p denotes the "classical radius" $(\frac{e^2}{M_o c^2})$ for the particle, and may be taken as 1.536×10^{-16} cm for a proton (rest mass equivalent to 938 Mev).

The shift of betatron frequency which results from the space-charge terms included in Eq. (5) is given by

$$\Delta(\nu_y^2) = K_E + K_M + K_S \tag{7}$$

and leads to the space-charge limit

$$N = B\frac{\pi}{2}\frac{b(a+b)}{r_p R}\frac{\nu_{y_o}^2 - \nu_y^2}{1 + \frac{b(a+b)}{h^2}\left[\epsilon_1(1 + B\beta^2\gamma^2) + \epsilon_2 B\beta^2\gamma^2(h^2/g^2)\right]}\beta^2\gamma^3 \tag{8a}$$

$$= B\frac{\pi}{2}\frac{h^2}{r_p R}\frac{\nu_{y_o}^2 - \nu_y^2}{\epsilon_1\left(B + \frac{1}{\beta^2\gamma^2}\right) + \epsilon_2 B\frac{h^2}{g^2} + \frac{h^2}{b(a+b)}\frac{1}{\beta^2\gamma^2}}\gamma \tag{8b}$$

$$= \frac{\pi}{2}\frac{h^2}{r_p R}\frac{\nu_{y_o}^2 - \nu_y^2}{\epsilon_1\left[1 + \frac{1}{B(\gamma^2 - 1)}\right] + \epsilon_2\frac{h^2}{g^2} + \frac{1}{B(\gamma^2 - 1)}\frac{h^2}{b(a+b)}}\gamma\,, \tag{8c}$$

in which ν_y refers to the frequency (oscillations per revolution) of the nearest axial betatron oscillation resonance, below the low-intensity value, to which the oscillation may be shifted. The form of the Eq. (8a) is most

suitable for indicating the correction factor,

$$F = \left\{1 + \frac{b(a+b)}{h^2}\left[\epsilon_1(1 + B\beta^2\gamma^2) + \epsilon_2 B\beta^2\gamma^2(h^2/g^2)\right]\right\}^{-1}, \qquad (9)$$

that must be applied to the usual formula for the space-charge limit of an isolated beam, but the form of Eq. (8c) may be more convenient for computation (when $h^2/ab < B\gamma^2$) and indicates more clearly the following characteristics of the transverse space-charge limit at high energy:

(i) The space-charge limited intensity becomes substantially proportional to γ;

(ii) The aperture dimensions become more important, and the beam dimensions correspondingly less so, in determining the space-charge limit; and

(iii) The bunching factor (B) becomes relatively less important [due to the almost complete elimination of 1/B from the sum of the coefficients K_E and K_S, given respectively by Equations (6a) and (6c), when β^2 is near unity and by virtue of the identity of the image-force coefficients (ϵ_1) that appear in these equations].

3. The Image-Force Coefficients

The image-force coefficients, ϵ_1 and ϵ_2, which have been introduced in Equations (6a-c), can be evaluated directly by the use of image charges or currents in certain simple two-dimensional configurations, and in other two-dimensional cases use may be made of conformal transformations to obtain an equivalent problem for which the solution by image techniques or other means is readily apparent.

a. The electrostatic image coefficient, ϵ_1

(1) Plane-parallel conducting surfaces

The simplest configuration for the electrostatic problem - and hence also for the equivalent problem concerning the ac magnetic field, in which the boundary conditions are satisfied by virtue of skin-effect currents induced in the conducting surfaces - is evidently that of two infinite parallel conducting planes, at elevations h above and below a line charge λ_1. The supplemental electric field at a point situated a distance y directly above the line charge can be obtained immediately by summing the effects produced by an infinite series of images, of alternating sign, or by use of a simple conformal transformation (Appendix B). The additional electric field at this point is vertically directed, of amount

$$E_{image} = \frac{\pi^2 \lambda_1}{12h^2} y \ , \tag{10}$$

and hence is in the same direction as the field $2\lambda_1/y$ which arises directly from a localized line charge. The coefficient ϵ_1, which was introduced in Eq. (4a), is thus seen to be

$$\epsilon_1 = \frac{\pi^2}{48} \tag{11}$$

for the boundary surfaces considered here.

(2) Elliptical boundary

It has been pointed out by Dr. John P. Blewett[6] that use of a conducting vacuum chamber with a circular cross section would provide the advantage

---

6. J.P. Blewett, private conversation (July, 1963).

of suppressing the coefficient ϵ_1 which otherwise is of major importance in determining the intensity limit which results from the requirement of single-particle stability. Since use of a chamber with a strictly circular cross section may prove inconvenient because of other practical design considerations, it is of interest to obtain the image-force coefficient for a chamber of elliptical cross section. Unfortunately, as will be seen, any substantial departure of the cross section from circularity results in the coefficient ϵ_1 assuming a value that is comparable to the value $\pi^2/48$ for the plane-parallel case. As will be noted in Section B, moreover, the image forces that arise from a coherent transverse displacement of the beam as a whole clearly will not vanish for a chamber of circular cross section.

The rather lengthy analysis of the image effects for an elliptical boundary, of semi-axes w (radially) and h (axially), has been outlined in Appendix D and leads to results expressible in terms of the complete elliptic integral $K(k)$ of the first kind and modulus k. The modulus k is to be selected so that

$$\frac{K'}{K} = \frac{2}{\pi} \tanh^{-1} \frac{h}{w} , \tag{12}$$

where K' denotes $K(k') = K(\sqrt{1 - k^2})$. In terms of this notation, the supplemental electric field at a distance y above a line charge at the center of the ellipse is

$$E_{image} = \frac{2\lambda_1}{3(w^2 - h^2)} \left[\frac{2(2 - k^2)K^2}{\pi^2} - 1\right] y , \tag{13}$$

and the image-force coefficient accordingly is

$$\epsilon_1 = \frac{1}{6[(w/h)^2 - 1]} \left[\frac{2(2 - k^2)K^2}{\pi^2} - 1\right] . \tag{14}$$

This result includes, as limiting cases, the results for the case of parallel planes and for a circular cylinder; approximate values of the coeffficient ϵ_1 for certain special cases of the axis ratio are listed in Table I below (see also Fig. 1).

TABLE I

Values of the electrostatic image coefficient ϵ_1 for a cylinder of elliptical cross section

w/h	k^2	ϵ_1
1	0	0
5/4	0.838	0.090
4/3	0.904	0.107
3/2	0.965_5	0.134
2/1	0.998	0.172
oo	1	$\frac{\pi^2}{48} \doteq 0.20562$

b. The magnetostatic image coefficient, ϵ_2

(1) Plane-parallel magnet poles

For extended plane ferromagnetic poles, the magnetostatic image coefficient ϵ_2 can be obtained immediately by summing the effects produced by an infinite set of current images of identical sign, or by use of a simple conformal transformation (Appendix C). The additional magnetic field at a point y directly above a line current I_1 is parallel to the pole surface and is oppositely directed to the field $2I_1/y$ (e.m.u.) which arises from the line current alone. The strength of the supplemental

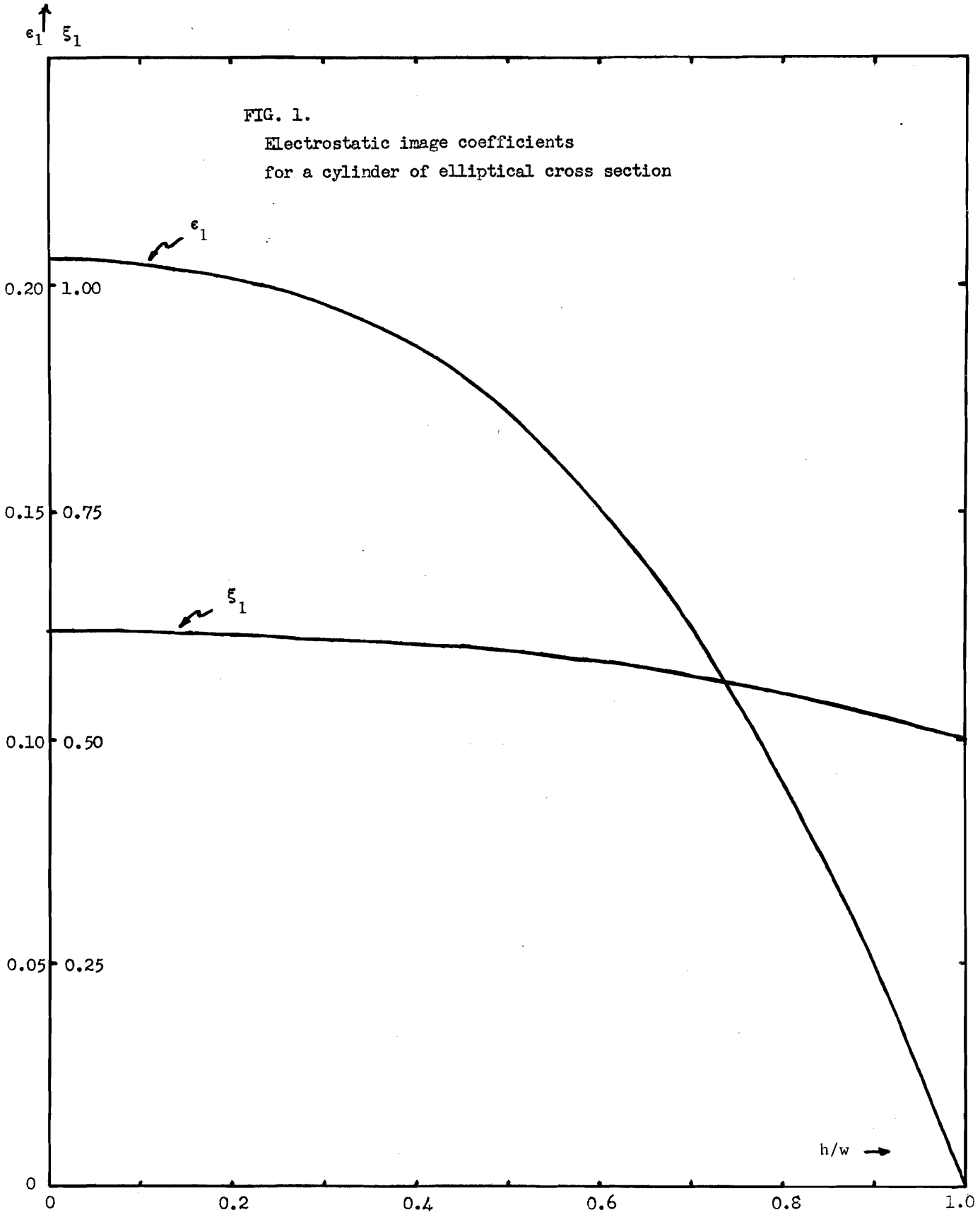

FIG. 1.
Electrostatic image coefficients
for a cylinder of elliptical cross section

field is

$$H_{image} = \frac{\pi^2 I_1}{6\, g^2}\, y \ . \qquad (15)$$

The image-force coefficient ϵ_2, which was first introduced in Eq. (4b'), accordingly becomes

$$\epsilon_2 = \frac{\pi^2}{24} \qquad (16)$$

for the boundary surfaces considered here.

(2) Wedge-shaped magnet gap

Since in practice the magnet poles are commonly designed to provide a magnetic field whose strength in the median plane is characterized by a substantial gradient (field index, $n \equiv -\frac{R}{H}\frac{dH}{dr}$), it is of interest to investigate whether the value of ϵ_2 is markedly modified in such circumstances. The detailed equations for the magnetic field generated by the beam may be different in form for various geometrical arrangements of the ferromagnetic material, and, in special cases, application of the usual boundary condition $H_t = 0$ may be incompatible with the necessary condition $\oint \vec{H}\cdot d\vec{\ell} = 4\pi\, \Sigma I$. In particular, it is found that, in addition to the expected radial component of field above and below the beam, an axial field component which effectively is independent of position may arise if the presence of the magnet yoke or some other feature of the geometrical configuration produces a lack of symmetry with respect to a vertical plane through the beam.*

---

*The presence of a substantially constant magnetic field component, typically given approximately by $\frac{\pi I_1}{g}\,\hat{\jmath}$, may be noted in the work of van Bladel (op. cit.,[5] Sect. III), wherein an image-field component of $\pi\hat{\jmath}$ gauss is shown in the neighborhood of a 50-amp beam (I_1 = 5 e.m.u.) when g = 5 cm. In this same report van Bladel investigates, evidently successfully, means of compensating the total image field in the median plane.

A rather simple magnet configuration for the production of a non-uniform field is that represented by a wedge-shaped gap, of half-angle α, with the beam current situated a distance X from the vertex of the wedge. The distance X may be identified with the reciprocal of the relative field gradient,

$$X = -\frac{H}{dh/dr} = \frac{R}{n} , \tag{17a}$$

and α may be related to the half-gap at the beam location by the equation

$$\alpha = \tan^{-1}\frac{g}{X} = \tan^{-1}\frac{g}{R/n} . \tag{17b}$$

By an analysis outlined in Appendix E, one finds an image field given by

$$\vec{H}_{image} = \frac{I_1}{X}\left\{\left(\frac{\pi}{\alpha} - 1\right)\left(\frac{\pi}{\alpha} - 5\right)\frac{y}{6X}\,\hat{i} + \left(\frac{\pi}{\alpha} - 1\right)\left[1 + \left(\frac{\pi}{\alpha} - 5\right)\frac{x}{6X}\right]\hat{j}\right\} \tag{18a}$$

$$\doteq I_1\left\{\pi^2\left[1 - \frac{6}{\pi}\left(\frac{g}{R/n}\right) + \left(\frac{2}{3} + \frac{5}{\pi^2}\right)\left(\frac{g}{R/n}\right)^2\right]\frac{y\hat{i} + x\hat{j}}{6g^2}\right.$$

$$\left. + \pi\left[1 - \frac{1}{\pi}\left(\frac{g}{R/n}\right) + \frac{1}{3}\left(\frac{g}{R/n}\right)^2\right]\frac{1}{g}\,\hat{j}\right\} .* \tag{18b}$$

Since the image coefficient ϵ_2 serves to characterize the horizontal component of the image field at points directly above the beam, we obtain

$$\epsilon_2 = \left(\frac{\pi}{\alpha} - 1\right)\left(\frac{\pi}{\alpha} - 5\right)\frac{g^2}{24X^2} \tag{19a}$$

$$\doteq \frac{\pi^2}{24}\left[1 - \frac{6}{\pi}\left(\frac{g}{R/n}\right) + \left(\frac{2}{3} + \frac{5}{\pi^2}\right)\left(\frac{g}{R/n}\right)^2\right] . \tag{19b}$$

Typically $g \ll R/n$ $(\alpha \ll 1)$ and the coefficient ϵ_2 then becomes substantially $\pi^2/24$, in agreement with the result obtained in sub-section (1) for plane-parallel magnet poles.

---

*The presence of a constant field component approximately given by $\frac{\pi I_1}{g}\,\hat{j}$ for $g \ll R/n$, of which mention was made in the footnote on p. 337, is evident from Eq. (18b).

(3) Other pole configurations

Other idealized two-dimensional pole configurations also are susceptible to analysis. The results would be of interest in permitting a comparison to be made between the image fields which arise in such cases and those present in the wedge-shaped gap that was considered in the preceding sub-section. In order that the gradient will be substantially constant over a limited region in the neighborhood of the beam, it might be considered desirable to locate the beam at a point of inflection for the median-plane magnetic field that is produced by the application of a magnetomotive force between the poles. Poles formed by two parallel circular cylinders of ferromagnetic material afford the advantage of permitting one to select independently both the semi-aperture (g) and the relative gradient (n/R), while locating the beam at a point of inflection for the median-plane field.[7] Such a pole system suffers, however, from the omission of a yoke structure to connect the two cylinders, as would be desirable in any practical application of this arrangement, and detailed analysis of the image fields for this case appears to require, moreover, a formidable amount of algebraic work.

Another pole configuration of possible interest for checking the results found for the wedge-shaped gap is that in which the pole surfaces are described by the hyperbolic cylinders $y^2 - x^2 = s^2$ (asymptotes at $\pm 45^o$) and by the vertical plane $x = 0$. For determining the image fields for the general case in which a line current is located at the point (X,y), it would be convenient to average the results for the following two cases: (i) line

---

7. The magnetic field produced by a specified magnetomotance applied between the cylinders may be evaluated in a manner similar to that appropriate for an analogous electrostatic problem discussed by Smythe: W.R. Smythe, "Static and Dynamic Electricity" (McGraw-Hill Book Company, Inc., New York, 1950) 2nd Ed., Sect. 4.17, pp. 80-82.

currents I_1 at (X,y) and at (X,-y); and (ii) a line current I_1 at (X,y) and $-I_1$ at (X,-y). Analysis of this problem again involves considerable algebraic effort, but for the simplified case in which the beam and field point are located in the median plane, at $X + \delta_1$ and $X + \delta$ respectively, the image field can be shown to be

$$\vec{H}_{image} = \frac{I_1}{X}\left[\frac{s^2 + 3X^2}{s^2 + X^2} - \frac{1}{2}\left(\frac{s^2 - X^2}{s^2 + X^2}\right)^2 \frac{\delta}{X} - \frac{1}{2}\,\frac{s^4 + 2X^2s^2 + 5X^4}{(s^2 + X^2)^2}\,\frac{\delta_1}{X}\right]\hat{j}\,, \qquad (20a)$$

for δ and δ_1 small. Application of the condition $\nabla \times \vec{H} = 0$ permits generalization of Eq. (20a) to include the case in which the field point is located a small distance, y, from the x-axis:

$$\vec{H}_{image} = \frac{I_1}{X}\left[\frac{s^2 + 3X^2}{s^2 + X^2}\,\hat{j} - \frac{1}{2}\,\frac{s^4 + 2X^2s^2 + 5X^4}{(s^2 + X^2)^2}\,\frac{\delta_1}{X}\,\hat{j} - \frac{1}{2}\left(\frac{s^2 - X^2}{s^2 + X^2}\right)^2 \frac{y\hat{i} + \delta\hat{j}}{X}\right], \qquad (20b)$$

for $y_1 = 0$. In limiting cases, Eq. (20b) may be simplified to

$$\vec{H}_{image} \doteq \frac{I_1}{X}\left[\hat{j} - \frac{y\hat{i} + (\delta + \delta_1)\hat{j}}{2X}\right], \qquad \text{for } s \gg X\,; \qquad (20b')$$

$$\vec{H}_{image} \doteq \frac{I_1}{X}\left[3\hat{j} - \frac{y\hat{i} + (\delta + 5\delta_1)\hat{j}}{2X}\right], \qquad \text{for } s \ll X\,. \qquad (20b'')$$

The results expressed by Equations (20b') and (20b'') are consistent with those given for a wedge-shaped gap by Eq. (E.4a) of Appendix E, if in these respective cases we set the half-angle α equal to $\pi/2$ or $\pi/4$, and if we identify x with δ, x_1 with δ_1, and set y_1 equal to zero. The image-force coefficient, ϵ_2, accordingly assumes the value $-\frac{g^2}{8X^2}$ in these limiting cases, as follows from Eq. (19a) with the substitution of $\pi/2$ or $\pi/4$ for α; in cases of practical importance, however, α would be taken as small ($g \ll R/n$) and interest would be directed to the dominant term of Eq. (19b).

B. Stability with Respect to a Collective Transverse Displacement

1. The Assumed Fields

In examining the stability of the beam with respect to a transverse displacement of the beam as a whole, it again is appropriate to consider separately the electrostatic field, the dc component of the magnetic field, and the ac magnetic field which occur in the presence of conducting or ferromagnetic boundaries. We now require these components of the image fields at a point x,y which coincides with the location of a displaced beam ($x_1 = x$, $y_1 = y$). We shall characterize these image fields by coefficients, ξ_1 and ξ_2, which, for consistency with the notation of Section A, are defined as follows in terms of the axial component of electric field from a line charge λ_1 and the radial component of magnetic field from a dc current I_1:

$$E_y = 4 \lambda_1 \xi_1 \frac{y}{h^2} , \tag{21a}$$

$$H_x = 4 I_1 \xi_2 \frac{y}{g^2} . \tag{21b}$$

2. The Equation of Motion

In a manner analogous to the procedure followed in Section A2, especially Equations (5) and (6a-c), we write the differential equation for axial betatron oscillation of the beam centroid as

$$\frac{d^2y}{d\theta^2} + (n + K'_E + K'_M + K'_S)\, y = 0 \tag{22}$$

where

$$K'_E = - \frac{2}{\pi} \frac{1}{B} \frac{N r_p R}{\beta^2 \gamma h^2} \xi_1 \tag{23a}$$

$$K'_M = -\frac{2}{\pi}\,\frac{N\,r_p\,R}{\gamma\,g^2}\,\xi_2 \tag{23b}$$

$$K'_S = \frac{2}{\pi}\left(\frac{1}{B} - 1\right)\frac{N\,r_p\,R}{\gamma\,h^2}\,\xi_1\ . \tag{23c}$$

By again identifying $\Delta(\nu_y^2)$ with $K'_E + K'_M + K'_S$, one obtains the space-charge limit imposed by the requirement of axial stability for coherent transverse motion:

$$N = \frac{\pi}{2}\,\frac{h^2}{r_p\,R}\,\frac{\nu_{y_o}^2 - \nu_y^2}{\xi_1\left[1 + \dfrac{1}{B(\gamma^2 - 1)}\right] + \xi_2(h^2/g^2)}\,\gamma\ .^{*} \tag{24}$$

The result expressed by Eq. (24) is clearly of the same form as Eq. (8c) when the self-field term $\dfrac{1}{B(\gamma^2 - 1)}\cdot\dfrac{h^2}{b(a+b)}$ is omitted from the denominator; as will be pointed out in the following sub-section, the numerical coefficients ξ_1 and ξ_2 will differ, however, from the coefficients ϵ_1 and ϵ_2 that are employed in Eq. (8c). Nevertheless, to the extent that the coefficients ξ_1, ξ_2 and ϵ_1, ϵ_2 are of a similar order of magnitude, the coherent and incoherent space-charge limits that are respectively expressed by Equations (24) and (8c) will be comparable when γ is large ($B\gamma^2 \gg h^2/ab$).

---

*If the beam location (y_1) is flopping on successive revolutions rapidly (in comparison to the leakage time for ac fields of such frequencies through the metallic chamber wall), the y_1-term in the so-called dc component of the magnetic field will be alternating also and would be subject to the boundary conditions imposed by the presence of the vacuum chamber. In this case we may replace g^2 by h^2 and ξ_2 by $-\xi_1$ in Eq. (24), with the result

$$N = \frac{\pi}{2}\,\frac{h^2}{r_p\,R}\,\frac{B}{\xi_1}\,(\nu_{y_o}^2 - \nu_y^2)\,\gamma\,(\gamma^2 - 1) \tag{24'}$$

$$= \frac{\pi}{2}\,\frac{h^2}{r_p\,R}\,\frac{B}{\xi_1}\,(\nu_{y_o}^2 - \nu_y^2)\,\beta^2\gamma^3 \tag{24''}$$

and note a consequent pronounced enhancement of the space-charge limit for stability of collective transverse motion. We are indebted to Dr. K.R. Symon for helpful discussion of this point.

3. The Image-Force Coefficients

a. The electrostatic image coefficient, ξ_1

(1) Plane-parallel conducting surfaces

The supplemental image field for a line charge λ_1 situated in a gap of height 2h between infinite parallel conducting planes can be derived directly by summing the contributions from an infinite series of images or by use of a simple conformal transformation. From the results of work described in Appendix B, the supplemental electric field is

$$E_y = \frac{\pi^2 \lambda_1}{12\, h^2} (y + 2y_1) \qquad (25a)$$

for a line charge (λ_1) displaced a distance y_1 from the median plane and the field point located directly above the charge at a distance y from the median plane. To obtain the image field at the center of the displaced beam, we set $y_1 = y$ and find

$$E_y = \frac{\pi^2 \lambda_1}{4\, h^2} y \,, \qquad (25b')$$

so that [see Eq. (21a)]

$$\xi_1 = \frac{\pi^2}{16} \,. \qquad (25b'')$$

It is noted that the value of ξ_1 given by Eq. (25b'') is three times the value of ϵ_1 given by Eq. (11) for the identical boundary configuration.

(2) Elliptical boundary

Similarly, with the notation introduced in sub-section A3a(2), the results of Appendix D lead to the following expression for the electric image field arising from small vertical displacements from the center of an elliptical conducting cylinder:

$$E_y = \frac{\lambda_1}{3(w^2 - h^2)} \left\{ 2 \left[\frac{2(2 - k^2)K^2}{\pi^2} - 1 \right] y + \left[\frac{4(1 + k^2)K^2}{\pi^2} - 1 \right] y_1 \right\} . \qquad (26a)$$

Again setting $y_1 = y$, this becomes

$$E_y = \frac{\lambda_1}{w^2 - h^2}\left[\frac{4K^2}{\pi^2} - 1\right] y \qquad (26b')$$

and

$$\xi_1 = \frac{1}{(w/h)^2 - 1}\left[\frac{K^2}{\pi^2} - \frac{1}{4}\right] . \qquad (26b'')$$

The result (26b') includes as a limiting case the image field which arises from the displacement of a line charge within a circular cylinder ($E_{image} = \frac{2\lambda_1}{h^2/y - y} \cong \frac{2\lambda_1}{h^2} y$, $\xi_1 = \frac{1}{2}$), and also that for infinite parallel conducting planes ($\xi_1 = \frac{\pi^2}{16}$, as obtained previously). Approximate values of the coefficient ξ_1 for certain special cases of the axis ratio are listed in Table II below:

TABLE II

Values of the electrostatic image coefficient ξ_1 for a cylinder of elliptical cross section

w/h	k^2	ξ_1
1	0	0.5
5/4	0.838	0.553
4/3	0.904	0.559
3/2	0.965_5	0.575
2/1	0.998	0.599
∞	1	$\frac{\pi^2}{16} \doteq 0.61685$

A remarkably small variation of ξ_1 is evident from the values given in Table II and from the graph shown in Fig. 1.

b. The magnetostatic image coefficient, ξ_2

(1) Plane-parallel magnet poles

The supplemental image field for a current I_1 situated in a gap of height 2g between infinite plane-parallel ferromagnetic slabs can be derived immediately by summing the contributions from an infinite set of images or by use of a simple conformal transformation. From the results of work described in Appendix C, the supplemental magnetic field is

$$H_x = \frac{\pi^2 I_1}{12\, g^2} (2y + y_1) \tag{27a}$$

for a current (I_1) displaced a distance y_1 from the median plane and the field point located directly over this current at a height y above the median plane. To obtain the image field at the center of the displaced beam, we set $y_1 = y$ and find

$$H_x = \frac{\pi^2 I_1}{4\, g^2}\, y\ , \tag{27b'}$$

so that [see Eq. (21b)]

$$\xi_2 = \frac{\pi^2}{16}\ . \tag{27b''}$$

It is noted that the value of ξ_2 given by Eq. (27b") is three-halves the value of e_2 given by Eq. (16) for the identical pole configuration.

(2) Wedge-shaped magnet gap

With the same notation as employed in sub-section A3b(2), the results of Appendix E lead to the following expression for the image field arising from small vertical displacements from the central plane of a wedge-shaped magnet gap:

$$\vec{H}_{image} = \frac{I_1}{X}\left\{\left(\frac{\pi}{\alpha} - 1\right)\left(\frac{\pi}{\alpha} - 5\right)\frac{y}{6X}\,\hat{i} + \left[\left(\frac{\pi}{\alpha}\right)^2 + 2\right]\frac{y_1}{12\,X}\,\hat{i}\right.$$

$$\left. + \left(\frac{\pi}{\alpha} - 1\right)\,\hat{j} + \left(\frac{\pi}{\alpha} - 1\right)\left(\frac{\pi}{\alpha} - 5\right)\frac{x}{6X}\,\hat{j} - \left[\left(\frac{\pi}{\alpha}\right)^2 - 1\right]\frac{x_1}{6X}\,\hat{j}\right\} \quad (28a)$$

$$\doteq I_1\left\{\frac{\pi^2}{6}\left[1 - \frac{6}{\pi}\left(\frac{g}{R/n}\right) + \left(\frac{2}{3} + \frac{5}{\pi^2}\right)\left(\frac{g}{R/n}\right)^2\right]\frac{y}{g^2}\,\hat{i}\right.$$

$$+ \frac{\pi^2}{12}\left[1 + 2\left(\frac{1}{3} + \frac{1}{\pi^2}\right)\left(\frac{g}{R/n}\right)^2\right]\frac{y_1}{g^2}\,\hat{i}$$

$$+ \pi\left[1 - \frac{1}{\pi}\left(\frac{g}{R/n}\right) + \frac{1}{3}\left(\frac{g}{R/n}\right)^2\right]\frac{1}{g}\,\hat{j}$$

$$+ \frac{\pi^2}{6}\left[1 - \frac{6}{\pi}\left(\frac{g}{R/n}\right) + \left(\frac{2}{3} + \frac{5}{\pi^2}\right)\left(\frac{g}{R/n}\right)^2\right]\frac{x}{g^2}\,\hat{j}$$

$$\left. - \frac{\pi^2}{6}\left[1 + \left(\frac{2}{3} - \frac{1}{\pi^2}\right)\left(\frac{g}{R/n}\right)^2\right]\frac{x_1}{g^2}\,\hat{j}\right\}, \quad (28b)$$

where the coordinates of the current and field point are respectively $(X + x_1, y_1)$ and $(X + x, y)$ with respect to the vertex of the wedge, X is identified as R/n, and $\alpha = \tan^{-1} g/X = \tan^{-1}\frac{g}{R/n}$ [Equations (17a-b)].

The terms of interest for determination of ξ_2 are those which involve y and y_1 ; with y_1 set equal to y, we obtain

$$H_x = \frac{I_1}{4X^2}\left[\left(\frac{\pi}{\alpha}\right)^2 - 4\left(\frac{\pi}{\alpha}\right) + 4\right] y \quad (29a)$$

$$\doteq \frac{\pi^2 I_1}{4\,g^2}\left[1 - \frac{4}{\pi}\left(\frac{g}{R/n}\right) + 2\left(\frac{1}{3} + \frac{2}{\pi^2}\right)\left(\frac{g}{R/n}\right)^2\right] y \quad (29b)$$

and

$$\xi_2 = \frac{1}{16}\left[\left(\frac{\pi}{\alpha}\right)^2 - 4\left(\frac{\pi}{\alpha}\right) + 4\right]\left(\frac{g}{X}\right)^2 \quad (30a)$$

$$\doteq \frac{\pi^2}{16}\left[1 - \frac{4}{\pi}\left(\frac{g}{R/n}\right) + 2\left(\frac{1}{3} + \frac{2}{\pi^2}\right)\left(\frac{g}{R/n}\right)^2\right] . \qquad (30b)$$

The dominant term in Eq. (30b) is seen to be in agreement with the value $\xi_2 = \pi^2/16$ that is given by Eq. (27b") for plane-parallel poles ($\frac{n}{R} \to 0$).

III. Examples

To illustrate the relative importance of energy and aperture in determining the transverse space-charge limit, numerical examples are presented in Table III for a proton synchrotron of 120 meters radius (as might be representative of an AGS designed for a final energy in the neighborhood of 30 or 35 Bev). The bunching factor, which plays an important role only at the lower energies, is taken somewhat arbitrarily as 3/8. The frequency of betatron oscillations is considered to be shifted by action of the space-charge forces from 8.75 oscillations per revolution to the half-integral resonant value of 8.50. Beam dimensions such that $b(a + b) = 5.25$ cm^2 are assumed, although these dimensions influence the results strongly only when the energy is low or the gap relatively large. The space-charge limits as determined by single-particle stability were computed by use of Eq. (8c) and the limits for the stability of coherent axial oscillation were evaluated by Eq. (24).* In all cases, plane-parallel magnet poles were assumed, so that $\epsilon_2 = \pi^2/24$ and $\xi_2 = \pi^2/16$.

---

*Since the space-charge limits given in Table I for stability of coherent beam displacement have been computed by use of Eq. (24), they may be considered as more representative of limits imposed by proximity to an integral resonance, for reasons indicated in the footnote to Eq. (24). In addition, considerations which have been carried out by the CERN group in regard to a multi-hundred Gev accelerator suggest that the bunching factor (B) necessarily will differ from unity by a greater amount than is the case in the example considered here.

TABLE III

Illustrative values of transverse space-charge limits, for protons[a]

B = 3/8, a = 2 cm, b = 1.5 cm, R = 12,000 cm, $\nu_{y_o}^2 - \nu_y^2 = (8.75)^2 - (8.50)^2 = 4.3125$

[The limiting number of particles is given by the values in the Table times 10^{14}.]

	Plane-Parallel Chamber			3:2 Chamber Aperture			Circular Chamber Aperture		
h = g:	3 cm	6 cm	10 cm	3 cm	6 cm	10 cm	3 cm	6 cm	10 cm
w:	∞	∞	∞	4.5 cm	9 cm	15 cm	3 cm	6 cm	10 cm
	Space-Charge Limit for Individual-Particle Stability								
ϵ_1:	---- $\pi^2/48 = 0.20562$ -----			--------- 0.134 ----------			---------- 0 ----------		
ϵ_2:	---- $\pi^2/24 = 0.41123$ -----			-------- 0.41123 ---------			-------- 0.41123 ---------		
$K.E._{inj.}$									
50 Mev	0.00735	0.00807	0.00824	0.00764	0.00815	0.00827	0.00826	0.00832	0.00833
200 Mev	0.0350	0.0396	0.0408	0.0365	0.0401	0.0409	0.0397	0.0410	0.0412
1 Bev	0.313	0.429	0.465	0.333	0.437	0.469	0.378	0.455	0.476
5 Bev	2.80	7.62	12.05	3.12	8.19	12.54	3.96	9.53	13.60
10 Bev	5.89	20.4	43.0	6.63	22.6	46.4	8.67	28.2	54.4
	Space-Charge Limit for Stability of Coherent Beam Displacement								
ξ_1:	---- $\pi^2/16 = 0.61685$ -----			--------- 0.575 ----------			---------- 0.5 ----------		
ξ_2:	---- $\pi^2/16 = 0.61685$ -----			-------- 0.61685 ---------			-------- 0.61685 ---------		
$K.E._{inj.}$									
50 Mev	0.0214	0.0857	0.238	0.0229	0.0917	0.255	0.0262	0.105	0.291
200 Mev	0.0850	0.340	0.945	0.0904	0.361	1.00	0.102	0.407	1.13
1 Bev	0.393	1.57	4.37	0.411	1.65	4.57	0.448	1.79	4.98
5 Bev	1.64	6.57	18.2	1.70	6.80	18.9	1.82	7.28	20.2
10 Bev	3.10	12.4	34.4	3.21	12.8	35.6	3.42	13.7	38.0

[a] $r_p = 1.536 \times 10^{-16}$ cm, for protons of rest mass equivalent to 938 Mev.
For the injection energies cited, we take γ respectively as 1.053, 1.213, 2.066, 6.330, and 11.66.

Several characteristic features of the space-charge phenomenon are apparent from the entries in Table III:

(i) At low energy, or for large apertures, the more stringent limitation is imposed by the requirement of single-particle stability, since the direct action of the beam fields on the particle is then dominant. At higher energies, when the image fields are of greater significance, the requirement for collective stability becomes the more important, since the image-field coefficients are greater for this case.

(ii) The number of particles is effectively proportional to $\beta^2\gamma^3$ only at the lower energies, but this dependence is followed over a somewhat more extended range of energy if the aperture is large. (Note, for example, that the ratio of $\beta^2\gamma^3$ for 200 Mev and 50 Mev kinetic energy is 4.96.) At high energies, the acceptable number of particles is substantially proportional to γ.

(iii) Similarly, the size of the aperture is of major importance at high energies, where the number of particles may vary directly as h^2. The shape of the vacuum-chamber aperture, however, does not appear from the examples considered ($h = g$) to be of great importance.

APPENDIX A

APPLICATION OF CONFORMAL TRANSFORMATIONS

In two-dimensional electrostatic problems, the method of conformal transformations employs a potential function that is the real or imaginary part of an analytic function ($W = U + iV$) of the complex position vector ($z = x + iy$). By virtue of the Cauchy-Riemann conditions, the potential (U or V) satisfies the two-dimensional Laplace equation, and the magnitude of the electric field strength is given by

$$E = \left|\frac{dW}{dz}\right| \quad . \tag{A.1}$$

If, for an isolated line charge of strength λ (e.s.u. per cm), we take $W = -2\lambda \log z$ (where z denotes the position of the field point with respect to the line charge), the potential function is*

$$\text{Potential} = U = -2\lambda \log |z| \quad , \tag{A.2a}$$

$$\vec{E} = -\text{ grad } U = 2\lambda \frac{\hat{r}}{r} \quad , \text{ and} \tag{A.2b'}$$

$$|E| = \frac{2\lambda}{r} = \left|\frac{dW}{dz}\right| . \tag{A.2b''}$$

With steady line currents in a two-dimensional problem, the Cartesian magnetic-field components and the vector potential (A, with $\vec{A} = A\hat{k}$) similarly satisfy the two-dimensional Laplace equation. Again a complex analytic function (W) may be employed, with $\vec{H} = \text{curl } \vec{A} = \hat{k} \times (-\text{grad A})$ and A expressed by U or V. For an isolated line current of strength I (e.m.u.), we may take $W = 2\,I \log z$, with

---

*We employ natural logarithms in this analysis.

$$A = U = -\,2\,I \log |z| \quad , \tag{A.3a}$$

$$\vec{H} = \hat{k} \times (-\text{grad } U) = 2\,I\,\frac{\hat{k} \times \hat{r}}{r}, \text{ and} \tag{A.3b'}$$

$$|H| = \frac{2I}{r} = \left|\frac{dW}{dz}\right| \text{ oersted.} \tag{A.3b''}$$

The usual boundary condition to be satisfied at the surface of ferromagnetic material of high permeability is $H_t = 0$, or $\partial A/\partial n = 0$ and the orthogonal function remains constant along the boundary. This requirement must be abandoned, however, if its application would violate the basic equation $\oint \vec{H} \cdot d\vec{\ell} = 4\pi \Sigma I$, as would be the case for a current-carrying conductor threading a tube of ferromagnetic material. The magnetic-field lines can be visualized as a system orthogonal to the flow lines in a current-flow or heat-flow problem in which, with similar geometry, the line current becomes a source and the ferromagnetic material assumes the property of very high resistance to the flow of current or heat. The magnetic-field lines are curves which then become, in this analogy, the electric or thermal equipotentials.

In the case of alternating currents, the phenomenon of skin effect will prevent the ac magnetic field from penetrating into neighboring conductors, and the magnetic field must be tangential at the surface of these conductors. The magnetic-field lines of a two-dimensional problem involving alternating currents directed exclusively in the z-direction thus constitute a system orthogonal to that given by the electric-field lines of the geometrically similar electrostatic problem, and the magnitude of the magnetic field will be just I/λ times the value of $\left|\frac{dW}{dz}\right|$ for the corresponding electrostatic case.

In all cases, determination of the complex function W may be aided by

use of intermediate conformal transformations in which the strength of the sources remains unchanged. Electrostatic field lines which go to infinity may, however, be interpreted as associated with a sink represented by a negative charge, and this charge will have to be included whenever the point at infinity is transformed to within the finite region of the next complex plane; an analogous situation in a magnetostatic problem would involve transforming a return current at infinity so that this current would fall in the finite region of the complex plane.

APPENDIX B

IMAGES IN INFINITE PARALLEL CONDUCTING PLANES

1. Application of Conformal Transformation

The transformation

$$z' = \exp \pi(z + ih)/2h \qquad (B.1)$$

is useful for transforming the boundaries of interest to the real axis of the z'-plane and carries the region between the plates into the upper half of this new complex plane.

z	z'
$\infty + ih$	$-\infty$
ih	-1
$-\infty$	0
$-ih$	$+1$
$\infty - ih$	$+\infty$

With the line charge λ_1 located at $z = iy_1$ and the field point at $z = iy$, the electrostatic potential may be written directly by use of a single image $(-\lambda_1)$ in the z_1-plane:

$$U = -2\lambda_1 \log \left| \frac{\exp i\pi(y + h)/2h - \exp i\pi(y_1 + h)/2h}{\exp i\pi(y + h)/2h - \exp -i\pi(y_1 + h)/2h} \right| \tag{B.2a}$$

$$= -2\lambda_1 \log \left| \frac{\sin \pi y/2h - \sin \pi y_1/2h}{1 + \cos \pi(y + y_1)/2h} \right| \tag{B.2b}$$

$$\doteq -2\lambda_1 \log \left\{ \frac{\pi}{4} \frac{|y - y_1|}{h} \left[1 + \frac{\pi^2}{48} \frac{y^2 + 4y\, y_1 + y_1^2}{h^2} \right] \right\} \tag{B.2c}$$

$$\doteq -2\lambda_1 \log \left(\frac{\pi}{4} \frac{|y - y_1|}{h} \right) - \frac{\pi^2 \lambda_1}{24\, h^2} (y^2 + 4yy_1 + y_1^2) \, . \tag{B.2d}$$

The image-field, as derived from the image-dependent term in Eq. (B.2d), then is

$$\vec{E}_{image} = \frac{\pi^2 \lambda_1}{12h^2} (y + 2y_1) \hat{j} \, , \qquad \text{for } x = x_1 \, . \tag{B.3}$$

This result is employed in the body of the present report in writing Equations (10) and (25a).

2. Direct Summation of Image Fields

The result expressed by Eq. (B.3) can be derived directly by summing the field contributions of an infinite series of images of alternating sign. The following system of images applies:

Charge	Distance from Field Point
Original λ_1	$y_1 - y$ above
$-\lambda_1$	$2h - y_1 - y$ above
$-\lambda_1$	$2h + y_1 + y$ below
$+\lambda_1$	$4h - y_1 + y$ below
$+\lambda_1$	$4h + y_1 - y$ above
$-\lambda_1$	$6h - y_1 - y$ above
$-\lambda_1$	$6h + y_1 + y$ below
...	...

The upward-directed electric field due to the images alone then is:

$$E_{image} = 2\lambda_1 \left[\frac{1}{2h-y_1-y} - \frac{1}{2h+y_1+y} + \frac{1}{4h-y_1+y} - \frac{1}{4h+y_1-y} + \frac{1}{6h-y_1-y} - \frac{1}{6h+y_1+y} + \ldots\right] \quad \text{(B.4a)}$$

$$= 4\lambda_1 \left[\frac{y_1 + y}{4h^2 - (y_1 + y)^2} + \frac{y_1 - y}{16h^2 - (y_1 - y)^2} + \frac{y_1 + y}{36h^2 - (y_1 + y)^2} + \ldots\right] \quad \text{(B.4b)}$$

$$\doteq \frac{\lambda_1}{h^2}\left\{\left[(y_1 + y) + (1/9)(y_1 + y) + (1/25)(y_1 + y) + \ldots\right] + \left[(1/4)(y_1 - y) + (1/16)(y_1 - y) + \ldots\right]\right\} \quad \text{(B.4c)}$$

$$= \frac{\lambda_1}{h^2}\left[(y_1+y)(1^{-2}+ 3^{-2}+ 5^{-2}+ \ldots) + (1/4)(y_1-y)(1^{-2}+ 2^{-2}+ 3^{-2} + \ldots)\right] \quad \text{(B.4d)}$$

$$= \frac{\lambda_1}{h^2}\left[(y_1 + y)\frac{\pi^2}{8} + (y_1 - y)\frac{\pi^2}{24}\right] \quad \text{(B.4e)}$$

$$= \frac{\pi^2\lambda_1}{12h^2}(y + 2y_1) , \quad \text{(B.4f)}$$

in agreement with Eq. (B.3).

APPENDIX C

IMAGES IN INFINITE PLANE-PARALLEL FERROMAGNETIC POLES

1. Application of Conformal Transformation

The field which arises from the images of a line current (I_1) in infinite plane-parallel ferromagnetic poles can be computed readily by aid of the transformation (B.1) that was introduced in Appendix B. The single image ($-\lambda_1$), which was employed in the z'-plane for the purpose of the electrostatic computation, now becomes replaced by a positive line current ($+I_1$). In addition, however, a line current $-I_1/2$ at $x = -\infty$ in the z-plane is transformed to $z' = 0$. This current, together with its image (of like sign) in the x'-axis, constitute a current ($-I_1$) whose contribution to the potential must be included. [The significance of the line current $-I_1/2$ at $x = -\infty$ may be appreciated most clearly by visualizing the analogous problem of conduction current or heat flow, in which half the flow lines emerging from the given source I_1 pass to the left to terminate on a "sink" (of source strength $-I_1/2$) at $x = -\infty$.]

With the line current I_1 located at $z = iy_1$ and the field point at $z = iy$, and with a pole separation of $2g$, the potential function becomes in this case:

$$A = U = -2\, I_1 \log \left| \frac{\left[\exp i\pi(y + g)/2g - \exp i\pi(y_1 + g)/2g\right] \times \left[\exp i\pi(y + g)/2g - \exp -i\pi(y_1 + g)/2g\right]}{\exp i\pi(y + g)/2g} \right| \qquad \text{(C.1a)}$$

$$= -2\, I_1 \log \left[2 \left| \sin \pi y/2g - \sin \pi y_1/2g \right|\right] \qquad \text{(C.1b)}$$

$$\doteq -2\, I_1 \log \left\{ \frac{\pi |y - y_1|}{g} \left[1 - \frac{\pi^2}{24} \frac{y^2 + yy_1 + y_1^2}{g^2} \right] \right\} \qquad \text{(C.1c)}$$

$$\doteq -2\, I_1 \log \left(\pi \frac{|y - y_1|}{g} \right) + \frac{\pi^2 I_1}{12\, g^2} (y^2 + yy_1 + y_1^2) \,. \qquad \text{(C.1d)}$$

The image field, as obtained by evaluation of $\hat{k} \times (-\text{grad } U)$ for the image-dependent terms in Eq. (C.1d), is in the x-direction and of the amount

$$H_{image} = \frac{\pi^2 I_1}{12 g^2} (2y + y_1) , \qquad \text{for } x = x_1. \tag{C.2}$$

This result is employed in the body of the report in writing Equations (15) and (27a).

2. Direct Summation of Image Fields

As in the electrostatic problem for infinite plane-parallel conducting plates, the magnetostatic problem to which Eq. (C.2) applies also can be solved directly by summing the field contributions of an infinite series of images. The locations of the required image currents are the same as for the line charges considered in Sect. 2 of Appendix B, but in the present case the sign of each image is that of the original current $(+I_1)$.

The horizontal magnetic field of the images $(\vec{H} = H_x \hat{i})$ is

$$H_{image} = 2I_1 \left[\frac{1}{2g-y_1-y} - \frac{1}{2g+y_1+y} - \frac{1}{4g-y_1+y} + \frac{1}{4g+y_1-y} + \frac{1}{6g-y_1-y} - \frac{1}{6g+y_1+y} + \ldots\right] \tag{C.3a}$$

$$= 4I_1 \left[\frac{y_1 + y}{4g^2 - (y_1 + y)^2} - \frac{y_1 - y}{16g^2 - (y_1 - y)^2} + \frac{y_1 + y}{36g^2 - (y_1 + y)^2} + \ldots\right] \tag{C.3b}$$

$$\doteq \frac{I_1}{g^2} \Big\{\left[(y_1 + y) + (1/9)(y_1 + y) + (1/25)(y_1 + y) + \ldots\right] - \left[(1/4)(y_1 - y) + (1/16)(y_1 - y) + \ldots\right]\Big\} \tag{C.3c}$$

$$= \frac{I_1}{g^2} \left[(y_1 + y)(1^{-2} + 3^{-2} + 5^{-2} + \ldots) - (1/4)(y_1 - y)(1^{-2} + 2^{-2} + 3^{-2} + \ldots)\right] \tag{C.3d}$$

$$= \frac{I_1}{g^2} \left[(y_1 + y)\frac{\pi^2}{8} - (y_1 - y)\frac{\pi^2}{24}\right] \tag{C.3e}$$

$$= \frac{\pi^2 I_1}{12g^2} (2y + y_1) , \qquad \text{in agreement with Eq. (C.2).} \tag{C.3f}$$

APPENDIX D

ELECTROSTATIC IMAGES IN AN ELLIPTICAL CONDUCTING CYLINDER

We are concerned here with the image fields which arise from an elliptical conducting cylinder, of which the upper portion extends from the point A ($x = w$) through B ($y = h$) to A_1 ($x = -w$). The center is at the origin (0,0), and the foci F, F_1 are at $x = \pm\sqrt{w^2 - h^2}$. Sufficient generality will be obtained for the work of this report by locating the line charge (λ_1) and the field point (F.P.) on the y-axis, at $z = iy_1$ and $z = iy$, respectively.

In order that specific boundary conditions may be applied along the line AA_1, despite the asymmetry introduced when $y_1 \neq 0$, it is convenient to consider the potential in the z-plane as the average of the potentials which would result in the following two cases:

Case I: The entire boundary, $OFABA_1F_1O$, of the region contained within the upper half of the ellipse is at constant (zero) potential.

Case II: The elliptical boundary is at constant (zero) potential, but the horizontal axis, AA_1 is a stream line.

These two cases would respectively arise if identical charges (λ_1) were located at $z = \pm iy_1$, or if charges of equal magnitude and opposite sign ($\pm\lambda_1$) were located at these two symmetrical points. In either case, the portions of the y-axis from λ_1 to B and to 0 are stream lines.

The transformation

$$z' = m \sin^{-1} \frac{z}{\sqrt{w^2 - h^2}} \tag{D.1}$$

will transform the region within the upper half of the ellipse to that within a rectangle in the z'-plane. A second transformation,

$$z'' = q \, sn(\frac{2K}{\pi} \frac{z'}{m}, k) \tag{D.2a}$$

$$= q \, sn \, (\frac{2K}{\pi} \sin^{-1} \frac{z}{\sqrt{w^2 - h^2}} , k) , \tag{D.2a'}$$

in turn will transform this region to that above the x''-axis of the z''-plane. The boundary point B lies at $x'' = \pm \infty$, the points A and A_1 at $\pm p$, and the points F and F_1 at $\pm q$. In Equations (D.2a,a'), K denotes the complete elliptic integral of the second kind,

$$k \equiv q/p , \tag{D.2b}$$

and k is selected so that

$$\frac{K'}{K} = \frac{2}{\pi} \tanh^{-1} \frac{h}{w} . * \tag{D.2c}$$

---

*K' denotes K(k'), where $k' \equiv \sqrt{1 - k^2}$. [For numerical values and helpful relations concerning elliptic functions and integrals, see, for example, E. Jahnke and F. Emde, "Tables of Functions (Funktionentafeln)" (Dover Publications, New York, 1945), Chapters V and VI.]

Point	z	z'	z''
0	0	0	0
λ_1	iy_1	$\text{im } \sinh^{-1} \frac{y_1}{\sqrt{w^2 - h^2}}$	iy_1''
F.P.	iy	$\text{im } \sinh^{-1} \frac{y}{\sqrt{w^2 - h^2}}$	iy''
B	ih	$\text{im } \tanh^{-1} \frac{h}{w}$	$\pm\infty$
A, A_1	$\pm w$	$m\,(\pm\frac{\pi}{2} + i \tanh^{-1} \frac{h}{w})$	$\pm p$
F, F_1	$\pm\sqrt{w^2 - h^2}$	$\pm m \frac{\pi}{2}$	$\pm q$

The location of the field point in the z''-plane is given by

$$z'' = iy'' = q\ \text{sn}\left(\frac{2iK}{\pi} \sinh^{-1} \frac{y}{\sqrt{w^2 - h^2}},\ k\right) \tag{D.3a}$$

$$= iq\ \text{tn}\left(\frac{2K}{\pi} \sinh^{-1} \frac{y}{\sqrt{w^2 - h^2}},\ k'\right), \tag{D.3b}$$

and a similar equation relates the coordinates y_1'' and y_1 of the line charge. In Case I, for which the entire boundary, BA_1OAB is at zero potential, the required potential function can be written immediately in terms of the coordinates in the z''-plane:

$$U_I = -2\lambda_1 \log \left| \frac{y'' - y_1''}{y'' + y_1''} \right| . \tag{D.4}$$

For Case II, in which the line segment A_1F_1OFA is a stream line while the remainder of the x''-axis is at zero potential, additional transformations are required. A possible systematic procedure employs the following:

(i) the transformation

$$z''' = t\sqrt{(z''/y_1'')^2 + 1}\ , \tag{D.5}$$

to bring the charge λ_1 to the origin of the z'''-plane [with the result that the stream line from $z'' = iy_1''$ to the origin of the z''-plane becomes a portion ($-t \le x''' \le t$) of that segment (AA_1, between the points $x''' = \pm t\sqrt{(p/y_1'')^2 + 1}$) of the x'''-axis which constitutes a stream line]; an image charge, λ_1, should also be imagined as located at the origin, an infinitesimal distance below the x'''-axis, in order that the strength of the original source λ_1 be confined, as it should, to the upper half of the z'''-plane;

(ii) the transformation

$$z^{iv} = \frac{2u}{\pi}\sin^{-1}\frac{z'''/t}{\sqrt{(p/y_1'')^2 + 1}} \tag{D.6a}$$

$$= \frac{2u}{\pi}\sin^{-1}\sqrt{\frac{z''^2 + y_1''^2}{p^2 + y_1''^2}}\ , \tag{D.6b}$$

to fold upward by 90^o the zero-potential portions of the x'''-axis; and (iii) the transformation, analogous to that employed in Sect. 1 of Appendix B,

$$z^v = v\exp\left[i\frac{\pi}{2}\left(1 - \frac{z^{iv}}{u}\right)\right]\ , \tag{D.7}$$

to bring the vertical equipotentials that extend between $\pm i\infty$ at $x^{iv} = \pm u$ into coincidence with the entire x^v-axis. By Eq. (D.7), the z^v-coordinates of the line charge (strength $2\lambda_1$) and of the field point above it become respectively $z_1^v = iy_1^v = iv$ and $z^v = iy^v = iv\exp\frac{\pi}{2}\frac{y^{iv}}{u}$.

For Case II, therefore, the potential function may be written

$$U_{II} = -4\lambda_1 \log \left| \frac{y^v - v}{y^v + v} \right| \tag{D.8a}$$

$$= 4\lambda_1 \log \operatorname{ctnh} \frac{\pi}{4} \frac{y^{iv}}{u} \tag{D.8b}$$

$$= 4\lambda_1 \log \operatorname{ctnh} \left(\frac{1}{2} \sinh^{-1} \sqrt{\frac{y''^2 - y_1''^2}{p^2 + y_1''^2}} \right) \tag{D.8c}$$

$$= 4\lambda_1 \log \frac{\sqrt{p^2 + y''^2} + \sqrt{p^2 + y_1''^2}}{\sqrt{y''^2 - y_1''^2}} . \tag{D.8d}$$

By averaging the potentials U_I and U_{II}, given by Equations (D.4) and (D.8d), we obtain the result

$$U = \lambda_1 \log \left[\frac{y'' + y_1''}{y'' - y_1''} \left(\frac{\sqrt{p^2 + y''^2} + \sqrt{p^2 + y''^2}}{\sqrt{y''^2 - y_1''^2}} \right)^2 \right] , \tag{D.9a}$$

which may be expressed in terms of the coordinates y and y_1 in the original z-plane as

$$U = 2\lambda_1 \log \frac{\sqrt{k^2 \operatorname{tn}^2\left(\frac{2K}{\pi}\sinh^{-1} \frac{y}{\sqrt{w^2-h^2}}, k'\right) + 1} + \sqrt{k^2 \operatorname{tn}^2\left(\frac{2K}{\pi}\sinh^{-1} \frac{y_1}{\sqrt{w^2-h^2}}, k'\right) + 1}}{k \left[\operatorname{tn}\left(\frac{2K}{\pi}\sinh^{-1} \frac{y}{\sqrt{w^2-h^2}}, k'\right) - \operatorname{tn}\left(\frac{2K}{\pi}\sinh^{-1} \frac{y_1}{\sqrt{w^2-h^2}}, k'\right) \right]} \tag{D.9b}$$

The potential expressed by Eq. (D.9b) may be expanded,* noting that $k' \equiv \sqrt{1 - k^2}$, to give the result

$$U \doteq -2\lambda_1 \left\{ \log\left(\frac{kK}{\pi} \frac{y-y_1}{\sqrt{w^2-h^2}}\right) + \frac{1}{6(w^2-h^2)} \left[\left(\frac{2(2-k^2)K^2}{\pi^2} - 1\right) y^2 + \left(\frac{4(1+k^2)K^2}{\pi^2} - 1\right) yy_1 + \left(\frac{2(2-k^2)K^2}{\pi^2} - 1\right) y_1^2 \right] \right\} , \tag{D.9c}$$

and the vertical image field becomes

$$E_{image} = \frac{\lambda_1}{3(w^2-h^2} \left\{ 2\left[\frac{2(2-k^2)K^2}{\pi^2} - 1\right] y + \left[\frac{4(1+k^2)K^2}{\pi^2} - 1\right] y_1 \right\} , \tag{D.10}$$

as has been employed in writing Equations (13) and (26a) in the body of the report.

The results expressed by Eq. (D.10) may be checked for two limiting cases – that of parallel planes ($w \to \infty$), and that of a circular cylinder ($w \to h$). In the first of these,

$$k \doteq 1, \qquad K' \doteq \frac{\pi}{2}, \qquad \text{and} \quad K \cong \frac{\pi^2}{4} \frac{w}{h},$$

---

*$$\mathrm{sn}(u,k) \doteq u - \frac{k^2+1}{6} u^3 + \frac{k^4 + 14k^2 + 1}{120} u^5 ,$$

as may be obtained by expanding the elliptic integral

$$u = \int_0^{\mathrm{sn}\, u} \frac{dt}{\sqrt{1 - t^2}\sqrt{1 - k^2t^2}} .$$

Then

$$\mathrm{cn}(u,k) \doteq 1 - \frac{1}{2} u^2 + \frac{4k^2 + 1}{24} u^4$$

and

$$\mathrm{tn}(u,k) \doteq u - \frac{k^2 - 2}{6} u^3 + \frac{k^4 - 16k^2 + 16}{120} u^5 .$$

In expanding factors of the form $y'' - y_1''$, terms through third order must be retained, in order that terms of second order will remain in the expansion after $y - y_1$ has been factored out.

in order that $\frac{K'}{K}$ equal $\frac{2}{\pi}\tanh^{-1}\frac{h}{w} \doteq \frac{2}{\pi}\frac{h}{w}$. Then

$$E_{\substack{\text{image} \\ w \to \infty}} \to \frac{\lambda_1}{3w^2}\left\{\frac{\pi^2}{4}\frac{w^2}{h^2}\,y + \frac{\pi^2}{2}\frac{w^2}{h^2}\,y_1\right\} = \frac{\pi^2\,\lambda_1}{12\,h^2}\,(y + 2y_1)\ ,$$

in agreement with Eq. (B.3) or (B.4f) of Appendix B.

In the second limiting case,

$$k^2 \cong 8(w - h)/h, \qquad K' \cong \log\sqrt{\frac{2h}{w-h}}\ , \qquad \text{and} \quad K^2 \cong \frac{\pi^2}{4}\left(1 + \frac{k^2}{2}\right).$$

Then

$$E_{\substack{\text{image} \\ w \to h}} \to \frac{\lambda_1}{6h(w-h)}\left\{2\left[\left(1 - \frac{k^2}{2}\right)\left(1 + \frac{k^2}{2}\right) - 1\right] y + \left[\left(1 + k^2\right)\left(1 + \frac{k^2}{2}\right) - 1\right] y_1\right\}$$

$$= \frac{\lambda_1 k^2}{4h(w-h)}\,y_1 = \frac{2\lambda_1}{h^2}\,y_1\ ,$$

as is directly obtainable from calculation of the image field which results from an image charge situated a distance h^2/y_1 from the center of a circular cylinder of radius h [see the discussion in the text following Eq. (26b'')].

APPENDIX E

MAGNETIC IMAGES FOR A WEDGE-SHAPED GAP

We consider here a wedge-shaped gap, of half-angle α, between ferromagnetic poles. The reference point, which serves as the origin of the z-plane, is situated on the median plane of the gap a distance X from the vertex. The current (I_1) and field point will be located with respect to this reference point by coordinates, (x_1,y_1) or (x,y), which themselves are small in comparison to the half-gap

$$g = X \tan \alpha \ . \qquad \text{(E.1a)}$$

Since the magnetostatic potential which would be generated by a pair of magnet poles in this configuration is proportional to the angular coordinate taken about the vertex as a center,[8] the distance X would equal $- \left. \frac{H}{dH/dr} \right|_X$ and we may set

$$X = \frac{R}{n} \ , \qquad \text{(E.1b)}$$

where n is the so-called "field index" which measures the relative gradient of the magnetic field. With this simple pole configuration, however, the field gradient may not be as constant as would be desirable in practice, but the arrangement described may serve as a useful model for the investigation of image forces resulting from the presence of a line current in the magnet gap.

The transformation

$$z' = ia' \left(\frac{z}{X} + 1\right)^{\pi/2\alpha} \qquad \text{(E.2)}$$

will transform the region between the ferromagnetic boundaries into the upper half of the z'-plane, with the vertex of the wedge (z = -X) transformed to z' = 0 and the reference point to z' = iy' = ia'. The potential function then may be written

8. See, for example, Sir James Jeans, "The Mathematical Theory of Electricity and Magnetism" (Cambridge University Press, Cambridge, 1948), Sect. 318.

$$A = U = -2I_1 \log \left| \left[(x' + iy') - (x_1' + iy_1') \right] \left[(x' + iy') - (x_1' - iy_1') \right] \right| \quad \text{(E.3a)}$$

$$= -2I_1 \log \left\{ a'^2 \left| \left[(1 + \frac{x+iy}{X})^{\pi/2\alpha} - (1 + \frac{x_1+iy_1}{X})^{\pi/2\alpha} \right] \right.\right.$$

$$\left.\left. \times \left[(1 + \frac{x+iy}{X})^{\pi/2\alpha} + (1 + \frac{x_1-iy_1}{X})^{\pi/2\alpha} \right] \right| \right\} \quad \text{(E.3b)}$$

$$\doteq -2I_1 \log \left(\frac{\pi a'^2}{\alpha} \frac{\sqrt{(x-x_1)^2 + (y-y_1)^2}}{X} \right)$$

$$- I_1 \left\{ (\frac{\pi}{\alpha} - 1)\frac{x+x_1}{X} + (\frac{\pi}{\alpha} - 1)(\frac{\pi}{\alpha} - 5)\frac{x^2+x_1^2 - y^2-y_1^2}{12\,X^2} \right.$$

$$\left. - \left[(\frac{\pi}{\alpha})^2 - 1 \right] \frac{x\,x_1}{6\,X^2} - \left[(\frac{\pi}{\alpha})^2 + 2 \right] \frac{y\,y_1}{12X^2} \right\} . \quad \text{(E.3c)}$$

By forming $\hat{k}$ x (-grad U), one obtains the supplementary image field

$$\vec{H}_{image} = \frac{I_1}{X} \left\{ (\frac{\pi}{\alpha} - 1)(\frac{\pi}{\alpha} - 5)\frac{y}{6X}\,\hat{i} + \left[(\frac{\pi}{\alpha})^2 + 2 \right] \frac{y_1}{12\,X}\,\hat{i} \right.$$

$$\left. + (\frac{\pi}{\alpha} - 1)\,\hat{j} + (\frac{\pi}{\alpha} - 1)(\frac{\pi}{\alpha} - 5)\frac{x}{6X}\,\hat{j} - \left[(\frac{\pi}{\alpha})^2 - 1 \right] \frac{x_1}{6X}\,\hat{j} \right\} \quad \text{(E.4a)}$$

$$\doteq I_1 \left\{ \frac{\pi^2}{6} \left[1 - \frac{6}{\pi}(\frac{g}{R/n}) + (\frac{2}{3} + \frac{5}{\pi^2})(\frac{g}{R/n})^2 \right] \frac{y}{g^2}\,\hat{i} \right.$$

$$+ \frac{\pi^2}{12} \left[1 + 2(\frac{1}{3} + \frac{1}{\pi^2})(\frac{g}{R/n})^2 \right] \frac{y_1}{g^2}\,\hat{i}$$

$$+ \pi \left[1 - \frac{1}{\pi}(\frac{g}{R/n}) + \frac{1}{3}(\frac{g}{R/n})^2 \right] \frac{1}{g}\,\hat{j}$$

$$+ \frac{\pi^2}{6} \left[1 - \frac{6}{\pi}(\frac{g}{R/n}) + (\frac{2}{3} + \frac{5}{\pi^2})(\frac{g}{R/n})^2 \right] \frac{x}{g^2}\,\hat{j}$$

$$\left. - \frac{\pi^2}{6} \left[1 + (\frac{2}{3} - \frac{1}{\pi^2})(\frac{g}{R/n})^2 \right] \frac{x_1}{g^2}\,\hat{j} \right\} , \quad \text{(E.4b)}$$

where in going from Eq. (E.4a) to (E.4b) we have made use of Equations (E.1a) and (E.1b) to identify X with R/n and α with $\tan^{-1}\frac{g}{R/n}$, and have considered g small in comparison to R/n.

Equation (E.4a) may be checked in two limiting cases, of which the first is that for which $\alpha \to 0$ and $X \to \infty$ so that $\alpha X \to g$. Physically this corresponds to the magnet surfaces becoming the faces of plane-parallel poles, with a yoke situated at a great distance to the left. In this case the image field becomes

$$\vec{H}_{(i)} = I_1 \left\{ \left[\frac{\pi}{g} + \frac{\pi^2}{6} \frac{x - x_1}{g^2} \right] \hat{j} + \frac{\pi^2}{12} \frac{2y + y_1}{g^2} \hat{i} \right\} .$$

In this result the horizontal field component agrees with Equations (C.2) and (C.3f) of Appendix C, the term $\frac{\pi^2 I_1}{6\, g^2}(x - x_1)\, \hat{j}$ is consistent with the condition $\nabla \times \vec{H} = 0$, and the component $\frac{\pi I_1}{g}\, \hat{j}$ is the field expected from an infinite set of current images in the yoke (images separated vertically by $2g$ and situated a large distance to the left).

In the limiting case that $\alpha \to \frac{\pi}{2}$, the distance X represents the distance by which the reference point is located to the right of the face of an infinite plane slab of ferromagnetic material. The field given by Eq. (E.4a),

$$\vec{H}_{(ii)} = I_1 \left[\left(\frac{1}{X} - \frac{x + x_1}{2\, X^2}\right) \hat{j} - \frac{y - y_1}{2\, X^2} \hat{i} \right] ,$$

is just the field to be expected at a point $X+x$ to the right of the slab by virtue of an image current (I_1) situated a distance $X+x_1$ to the left of the slab when the difference in elevation is $y-y_1$:

$$\vec{H}_{(ii)} = 2I_1 \left[\frac{2X + x + x_1}{(2X + x + x_1)^2 + (y - y_1)^2} \hat{j} - \frac{y - y_1}{(2X + x + x_1)^2 + (y - y_1)^2} \hat{i} \right]$$

$$\doteq I_1 \left[\frac{1}{X} \left(1 - \frac{x + x_1}{2X}\right) \hat{j} - \frac{y - y_1}{2X^2} \hat{i} \right],$$

as was obtained from Eq. (E.4a) for the case $\alpha \to \frac{\pi}{2}$.